Highly selective photonic glass filter for saturated blue structural color

Cite as: APL Photonics 4, 046101 (2019); https://doi.org/10.1063/1.5084138
Submitted: 04 December 2018 . Accepted: 15 March 2019 . Published Online: 02 April 2019

Guoliang Shang, Yen Häntsch, Kaline Pagnan Furlan, Rolf Janßen, Gerold A. Schneider, Alexander Petrov, and Manfred Eich

Highly selective photonic glass filter for saturated blue structural color

Cite as: APL Photon. 4, 046101 (2019); doi: 10.1063/1.5084138
Submitted: 4 December 2018 • Accepted: 15 March 2019 •
Published Online: 2 April 2019

Guoliang Shang,[1,a),b)] Yen Häntsch,[2,a)] Kaline Pagnan Furlan,[2] Rolf Janßen,[2] Gerold A. Schneider,[2] Alexander Petrov,[1,3] and Manfred Eich[1,4]

AFFILIATIONS

[1]Institute of Optical and Electronic Materials, Hamburg University of Technology, Eissendorfer Strasse 38, 21073 Hamburg, Germany
[2]Institute of Advanced Ceramics, Hamburg University of Technology, Denickestrasse 15, 21073 Hamburg, Germany
[3]ITMO University, 49 Kronverkskii Ave., 197101 St. Petersburg, Russia
[4]Institute of Materials Research, Helmholtz-Zentrum Geesthacht, Max-Planck-Strasse 1, Geesthacht D-21502, Germany

[a)]**Contributions:** G. Shang and Y. Häntsch contributed equally to this work.
[b)]**Author to whom correspondence should be addressed:** guoliang.shang@tuhh.de

ABSTRACT

Angle independent non-absorbing spectral filters are required for many applications such as sunscreens, structural colors, photovoltaics, and radiative cooling. One of the promising and simple to manufacture structures is based on the disordered arrangement of monodisperse spherical particles by self-assembly, also called photonic glasses. So far, reported photonic glasses inherently show poor spectral selectivity with a smooth transition in reflection. No significant improvement is usually expected from particles optimization as the Mie resonances are broad for small dielectric particles with a moderate refractive index. Via Fourier space engineering, we show here that it is, nonetheless, possible to obtain sharp spectral transitions from the synergetic effect of a core-shell geometry of the particles with the short range order of the photonic glass. We apply the developed approach to demonstrate a high color saturation of a non-iridescent blue structural color employing a photonic glass with hollow sphere particles, which features a sharp spectral transition in reflection. The experimental results support the theoretical predictions from the first-order approximation.

I. INTRODUCTION

Angle independent (non-iridescent) non-absorbing spectral filters are required for many applications which can cover wavelength regions from ultraviolet (UV)[1] to mid-infrared (MIR).[2–4] To protect the human skin from sunburn by the UV radiation, sunscreens need to effectively block UV radiation, while being able to transmit visible light in order to avoid the unwanted whitening effect on the skin.[1] Moreover, it would be beneficial to have non-absorbing sunscreens, which would reflect UV rather than absorbing the radiation since this could lead to unwanted photocatalytic effects in the skin.[1] In addition, such selective reflecting structures could be bigger in size than the titania nanoparticles used today, which reduces the risk of nanoparticle uptake into the organism.[5] At visible wavelengths, angle independent spectral filters can be used to obtain non-iridescent structural colors by moving the reflection transition into the visible range.[2,6] Since conventional pigments derive their colors from selective light absorption which is connected to their chemical structure, a saturated color based on non-toxic materials of high UV and chemical stability has been difficult to achieve.[7,8] The promising alternative is non-iridescent structural colors based on spectrally selective light scattering from nanostructures, which depends only on the refractive index distribution and can be produced from non-absorbing and environmentally friendly materials[2,6] of high light-fastness. Furthermore, when the reflection edge is shifted to the infrared region, this concept can be further applied to avoid thermal cooling of an incandescent lamp, strongly improving its efficiency[3] or to reflect visible and near infrared radiation and transmit MIR thermal emission for day time radiative cooling.[4,9]

There is significant progress in designing non-iridescent spectrally selective surfaces by lithographic and thin film techniques.[10–13] At the same time, these techniques can neither be applied to arbitrary surfaces nor be applied on a technically relevant scale, as would be required for color or UV protection applications. Another approach to obtain spectrally selective scattering is based on large 10-100 μm sized agglomerates of submicrometer particles that demonstrate radial periodicity, also called spherical opals,[14–18] or opal periodicity, also called photonic polycrystals.[19–22] These agglomerates are much larger than the desired size of 0.1–1 μm for commercial pigments.[23,24] Here, we consider a structure based on the disordered arrangement of monodisperse spherical particles with the size range of 200-300 nm, also called photonic glass (PhG). The type of structures can be obtained directly as a coating on arbitrary surfaces[25,26] when the solvent is evaporated. PhG has attracted a lot of attention due to its straightforward production procedure.[25–33] Due to the disordered isotropic arrangement, the reflection of PhGs is independent of the angles of illumination and observation (non-iridescence). At the same time, full sphere PhGs inherently demonstrate poor spectral selectivity connected to the smooth transition in reflection.[26,29–35] The spectral response of photonic glasses is usually connected to the Mie resonances of single particles[27,36,37] and/or to the short range order in the PhG.[38–40] No significant improvement is expected from changing the refractive index of the particle material as the Mie resonances are broad for small dielectric particles with a moderate refractive index of common dielectric materials. Moreover, the short range order of a photonic glass alone is also insufficient to cause sharp spectral features.

Recently, we have introduced the first-order scattering approximation and Ewald sphere construction to analyze the reflection characteristics from a scatterer in the film geometry.[40,41] In a novel Fourier space engineering approach, we showed theoretically that the combination of a well-chosen motif geometry, namely, a non-monotonous refractive index distribution along the radial coordinate from the center of the particle core through the shell into the background material, with the short range order of a PhG has strong synergetic effects.[40] A sharp transition in the Fourier transform (FT) of the PhG structure could be obtained, which relates to a sharp transition in reflection thus in a high selectivity of the PhG as a spectral filter. This required sharp transition in the PhG FT was obtained by shifting the first zero position of just the motif FT to smaller wave numbers with respect to the fixed peak of the lattice FT, thereby pulling the complete PhG FT to zero along a much bigger slope. Now, we present the experimental realization of this concept and demonstrate its applicability on the example of a blue non-iridescent structural color. In our paper, we have experimentally realized the highly saturated blue structural color by co-assembling of yttria-stabilized zirconia (YSZ) nanoparticles. Based on our previously published theoretical results[40] and on the actual material choice, we have adjusted the sphere parameters in order to obtain the desired sharp transition in the reflection spectrum. The achieved color saturation for a non-iridescent structural color is very high compared to the values reported on other structural colors based on PhG from full dielectric spheres. These experimental results confirmed the applicability of the previously presented theoretical approach for the design of highly saturated structural colors based on PhG.

II. RESULTS AND DISCUSSION

The reflection of a disordered structure as a PhG [Fig. 1(a)] is determined from its scattering properties. The light scattering from a permittivity perturbation $\Delta\varepsilon(\vec{r})$ small with respect to the background level can be estimated from the first-order Born approximation,[42] where each infinitesimal volume of the perturbation represents a point source of scattered light. The emission of a set of such distributed sources in far field can be conveniently described in reciprocal space as distribution of excited wavevectors. This distribution is obtained as an overlap between the FT of the permittivity perturbation with a sphere which contains all possible scattering wavevectors, which, as the scattering is elastic, all must have the same magnitude. This sphere is called Ewald sphere. It is positioned at the starting point of the input wavevector $\vec{k}_{in}$, which has its end at the origin of the reciprocal space [Fig. 1(b)]. The length of $\vec{k}_{in}$ is defined as $n_b\omega/c$, where ω is the frequency, c is the speed of light in vacuum, and n_b is the refractive index of the background material. The Ewald sphere construction geometrically predicts the wavelength dependence of the power and the directions of the scattered light.[41,43] In our consideration, we are interested in analyzing the transition of the reflection from long wavelengths to short wavelength, where the first-order Born approximation is applicable. For the spectral region where the reflection becomes strong, the first-order approximation will fail. There, diffuse light propagation in PhG should be considered. In Figs. 1(a) and 1(b), it is possible to see how scattering directions change with wavelength. The reflected power P from a scattering volume increases proportionally to the square of the absolute value of FT of $\Delta\varepsilon(\vec{r})$ integrated over the Ewald sphere surface (ESS)[40,41]

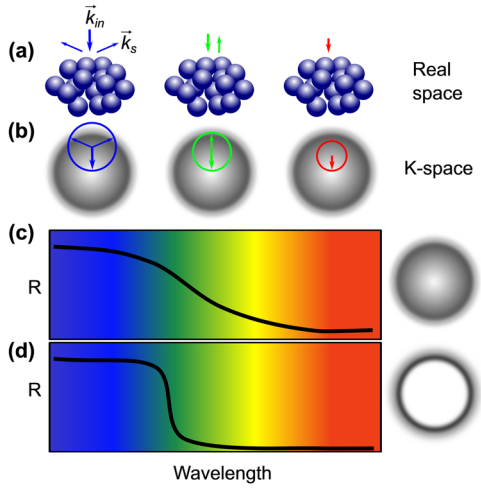

FIG. 1. The schematic representation of the Ewald sphere construction for reflection from PhG and corresponding schematic reflection spectra. (a) Light of different incident wavelengths scattered by the PhG into different wavevectors in real space. (b) The corresponding description in K-space using the Ewald sphere construction. The scattered wavevectors are obtained as intersection of Ewald sphere (sharp rings in red, green, and blue, depending on the wavelength of the incident light) with the absolute squared FT of the permittivity distribution (gray). The schematic reflection curves for the FT shell with (c) smooth and (d) sharp inner edges.

$$P = I_0 \frac{\omega^4}{16\pi^2 c^4} \int_{ESS} \frac{\left|\mathcal{F}\{\Delta\varepsilon(\vec{r})\}\left(\vec{k}\right)\right|^2}{k_s^2} g(\theta) d^2k, \quad (1)$$

where I_0 is the intensity of the incident plane wave of light, θ is the angle between scattered $\vec{k}_s$ and input $\vec{k}_{in}$ wavevectors, and for unpolarized light, $g(\theta) = (1 + \cos^2\theta)/2$. Thus, knowing $\vec{k}_{in}$, the light scattering can be analyzed from the FT of the permittivity. To obtain a sharp spectral transition, the radial function of the permittivity FT should also demonstrate a sharp transition starting from zero $\vec{k}$ to larger magnitudes [compare Figs. 1(c) and 1(d)].

The key scientific challenge arising from these findings is how to realize a structure with such a specific feature of its spatial FT. A PhG is a particular system which possesses only a near range positional order but no long range order in its lattice. Such a PhG can be described by its disordered lattice with short range order and a spherical particle as the motif. Since the scatterer structure can be interpreted as the convolution of the lattice with the motif in real space, mathematically, its FT is a multiplication of the lattice FT with the motif FT. Two normalized function are usually defined: the structure factor $\mathcal{S}$, containing the FT of the lattice, and the form factor $\mathcal{P}$ containing the FT of the motif. The square of the absolute value of the lattice FT averaged over all possible realizations and normalized by the number of lattice points is called structure factor $\mathcal{S}$, and the square of the absolute value of FT of the motif normalized by the motif volume (V) is called form factor $\mathcal{P}$. Thus, the average square of the absolute value of FT of the PhG structure with N particles is proportional to the multiplication of $\mathcal{S}$ and $\mathcal{P}$[40]

$$\left\langle |\mathcal{F}_t|^2 \right\rangle = \left\langle \mathcal{F}_t^2 \right\rangle = NV^2 \mathcal{S} \cdot \mathcal{P}. \quad (2)$$

The approximate function of radial distribution of $\mathcal{S}$ can be derived from solving the Ornstein-Zernike integral equation by choosing the hard sphere Percus-Yevick approximation.[40] It can be calculated for PhGs with different packing densities (ρ) defined as the volume fraction occupied by spheres. Here, we use ρ of 55%, which is an approximate of the value obtained experimentally from full sphere PhGs.[44]

Figure 2 shows the FTs of the full sphere and hollow sphere PhGs. The refractive indices are n = 1.6 (PS) for the full sphere, n_s = 1.8 for the shell (from YSZ nanoparticle) of the hollow sphere, and n_b = 1 for the background material (air). A slightly smaller refractive index of YSZ is taken as reported in the literature,[45] to account for the residual fine porosity of the shells composed of nanoparticles. As can be seen from Fig. 2(a), the first-zero point of the full sphere form factor is located at the right side of the lattice peak at $k_{lp} = 1.21(2\pi/a)$. The zero point of the form factor can be shifted to the left side of the lattice peak by motif engineering, as discussed in Ref. 40. The refractive index should change non-monotonously from the core of the particle through the shell into the background medium. Also, the shell thickness and the core diameter have to be adjusted. Here, a hollow sphere is designed which employs a ratio of the core to the whole sphere diameter (equal to the core diameter plus two times the shell thickness) of $d_c/d = 0.92$. This particular design of the motif moves the zero point of the motif FT right to the position left of the main peak of the structure factor, thereby pulling the product function $\mathcal{S} \cdot \mathcal{P}$ effectively to zero with the desired steep slope. The maximum of the $\mathcal{S} \cdot \mathcal{P}$ curve for the hollow sphere

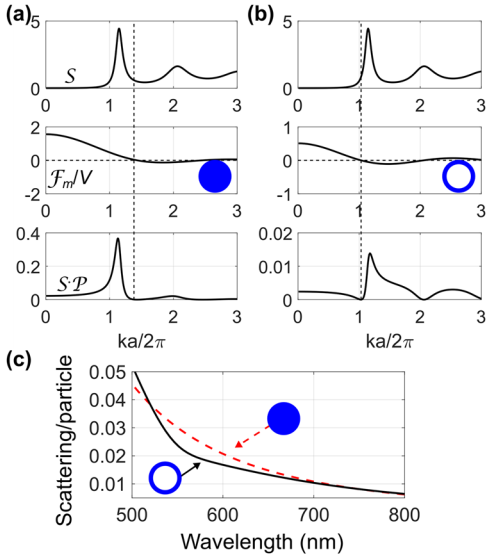

FIG. 2. FTs and scattering efficiency of the full sphere and hollow sphere PhGs. (a) and (b): Lattice structure factor $\mathcal{S}$ with ρ of 55% (top), normalized amplitude of the motif FT $\mathcal{F}_m/V$ (middle), presented as amplitude to easily track its zero points, and, in the third row, the product of $\mathcal{S}$ and $\mathcal{P}$ (bottom) as functions of the radial wavenumber k for PhGs made of (a) the full sphere and (b) the designed hollow sphere, respectively. The vertical black dashed lines indicate the zero position k_{m0} of the motif functions. The horizontal axis corresponding to the radial wavenumber is normalized by $2\pi/a$. (c) Scattering efficiency of the PhG per particle evaluated for the full sphere PhG (red dashed curve) and for the hollow sphere PhG (black solid curve), respectively.

case is much smaller than that for the full sphere case due to the large empty volume in the core. The wavelength of the scattering transition obtained from Eq. (1) is dependent on the average refractive index n_{av} of the PhG and on the sphere diameter $d = a$. The n_{av} of the hollow sphere PhG is smaller than that of the full sphere PhG. Thus the diameter of hollow spheres needs to be increased to match the transition wavelengths. Figure 2(c) shows the scattering cross section of the PhG per particle normalized by the particle geometrical cross section for the full sphere (d = 172 nm) PhG (red dashed curve) and the hollow sphere (d = 316 nm and d_c = 290 nm) PhG (black solid curve), respectively. The geometrical parameters are taken from experimentally realized structures, which are discussed later. We deliberately choose the size of the PS spheres for the full sphere PhG in the same range as reported in the literature to produce a blue color.[29,33] We adjust the hollow sphere size to have reflection transition at the same wavelength. As can be seen from Fig. 2(c), the hollow sphere PhG shows a steeper transition from low scattering to strong scattering in the spectral scattering efficiency than the full sphere PhG. The chosen sizes of full and hollow sphere particles result in comparable scattering strengths per particle.

Figure 3 shows the experimental structure of the PS full sphere PhG from particles with 172 nm diameter and the YSZ hollow sphere PhG with pores defined by PS particles of 295 nm diameter, respectively. The thickness of the full sphere PhG film is about 5.3 μm. For hollow sphere PhG, the resulting thickness of the YSZ shell is

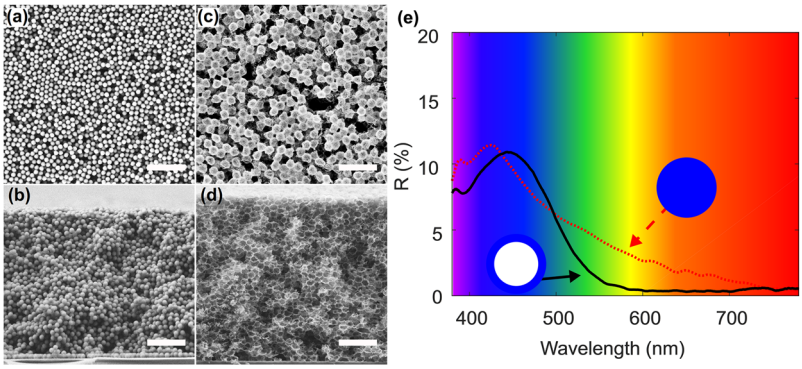

FIG. 3. Experimental structures and reflection spectra of the PS full sphere and the YSZ hollow sphere PhG. Top view (a) and the cross-sectional (b) SEM images of PS full sphere PhG. Top view (c) and the cross-sectional (d) SEM images of YSZ hollow sphere PhG. Scale bar is 1 μm. (e) The measured reflection spectrum of a 5.3 μm thick film of a PS full sphere PhG (red dotted curve) and of a 5.8 μm thick film of a YSZ hollow sphere PhG (black solid curve), respectively.

about 13 nm and the film thickness is around 5.8 μm. As can be seen from Figs. 3(a)–3(d), a disordered arrangement was obtained. The main parameter that defines the sharpness of the PhG structural factor is the packing density. For typical self-assembled structures, this packing density is around 55%.[44] For a smaller packing density, the main peak of the structure factor will broaden which will result in a reduced color saturation. Also, the peak will slightly shift to smaller wave numbers.[40] The light reflection spectra for the PS full sphere PhG (red dotted curve) and the YSZ hollow sphere PhG (black solid curve) are shown in Fig. 3(e). These light reflection spectra demonstrate the same feature as the calculated scattering efficiency [Fig. 2(c)]. The scattering per particle, derived from the first-order approximation, neglects the finite film thickness and multiple scattering events and thus gives the trend of the reflection transition but not the exact function. The hollow sphere PhG shows a much sharper transition in the reflection spectrum and thus a more saturated blue color in comparison with the PS full sphere PhG [Figs. 4(a) and 4(b)].

In Figs. 4(a) and 4(b), we show the colored areas of two samples [full sphere PhG (top) and hollow sphere PhG (bottom)] under identical imaging conditions. To demonstrate the non-iridescent properties, both samples are also tilted by 45° keeping the illumination condition fixed [Figs. 4(c) and 4(d)]. To prove that we observe structural color effect and not selective absorption, both samples are also imaged on white background [Figs. 4(e)–4(h)]. The color is almost absent as expected for structural colors due the fact that the transmitted spectrum is broadband back-reflected from the white surface. In the case of the black background, this transmitted part is broadband absorbed and thus only the part of the spectrum reflected from the PhG itself is observed, resulting in the structural color effect.

The corresponding CIE chromaticity diagram points were calculated based on the measured reflection spectra [Fig. 3(e)], as shown in Fig. 5. In such a diagram, a fully saturated color originating from monochromatic light can be found on the outer perimeter. A completely unsaturated color like gray or white is located in the so-called white point in the center of the diagram.[47] For the full sphere PhG, we are at x = 0.23 and y = 0.24, which is also comparable to the positions of the star [calculated from spectrum in Fig. 2(b)[33]], square [spectrum in Fig. 6(b)[26]], pentagon [spectrum in Fig. 3(b)[29]],

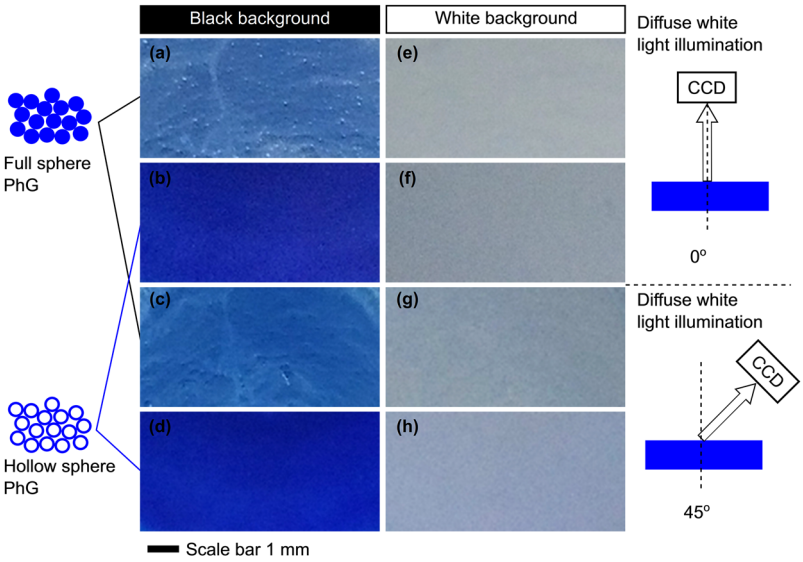

FIG. 4. Color impressions of the PS full sphere and YSZ hollow sphere PhG. The color expressions of the PS full sphere PhG (a) and YSZ hollow sphere PhG (b) viewed at an angle of 0° [(a) and (b)] and 45° [(c) and (d)], respectively. Images in each row represent the same sample with black [(a)–(d)] or white [(e)–(h)] background. The digital images of cm sized films of the PS full sphere PhG and the YSZ hollow sphere PhG are taken simultaneously to ensure the same diffuse illumination and viewing conditions for the color comparison.

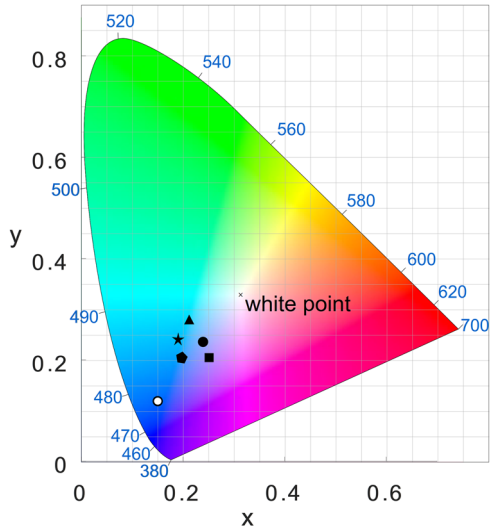

FIG. 5. CIE chromaticity diagram points. The resulting positions in CIE 1931 XYZ color space of the PS full sphere PhG (circle) and the YSZ hollow sphere PhG (hollow circle), respectively. For comparison, the color positions calculated from previously reported PhG spectra are also plotted as a star (PS full sphere, cuttlefish ink),[33] square (SiO_2 full sphere, carbon black),[26] pentagon (SiO_2 full sphere, carbon black),[29] and triangle [PS/poly(NiPAm-AAc) core-shell sphere].[46] The YSZ hollow sphere PhG based structural color is positioned much further away from the white point and much closer to the perimeter line of fully saturated (monochromatic) colors.

and triangle [spectrum in Fig. 3[46]] obtained from the literature. The positions from the literature are slightly further away from the white point than our full sphere PhG result, which is only possible in a light lossy structure with an added broad-band absorber which attenuates light having a greater penetration depth.[26,29,33] For the triangle point,[46] the core-shell sphere with a monotonically changing refractive index from core (PS) through the shell [poly(NiPAm-AAc) with a refractive index equal to water] into water as background was used for the blue color; therefore, color saturation is not improved. The hollow sphere PhG presented here is much further away from the white point with its sharp reflection edge yielding x = 0.15 and y = 0.13 and thus a more saturated blue color.

III. CONCLUSION

In conclusion, we devised a completely new design scheme based on Fourier space engineering for realizing non-absorbing non-iridescent spectral filters with high spectral selectivity based on disordered PhGs. While the non-iridescence stems from the disordered arrangement of the PhG, the high spectral selectivity is obtained by the optimization of the particle geometry in relation to the particle arrangement. In reciprocal space, the zero point of the particle permittivity distribution can be used to sharpen the transition from weak scattering to strong scattering. We show the applicability on the example of a blue non-iridescent structural color based on such a PhG from hollow YSZ spheres. The experimental results confirm the expectations from our first-order theoretical considerations. The achieved reflection transition is sharp for non-iridescent structural color with disordered structures, as shown by the comparison with other structural colors based on a PhG from full dielectric spheres. More generally, these results show that Fourier space engineering can significantly improve the selectivity of PhG based spectral filter structures. The hollow sphere PhG is made of YSZ which is a material stable at high temperatures up to 1000 °C. Taking into account that spectral characteristics of PhGs can be easily shifted with the diameter of the particles, the presented approach can also be applied for angle independent filters in UV sunscreens, photovoltaics, and radiative cooling.

IV. METHODS

A. Sample preparation

Crystalline YSZ nanoparticles with a diameter around 4 nm were synthesized by a hydrothermal synthesis method.[48] Briefly, an aqueous solution of zirconyl nitrate hydrate (0.1M), yttrium nitrate hexahydrate (0.05M), and acetylacetone (0.1M) was heated up to 160 °C for 3 days in an autoclave. The generated suspension was then dialyzed with ultrapure water using a tubular cellulose membrane. After centrifuging the purified YSZ suspension at 5000 × g for 1 h, the supernatant was removed. The YSZ suspension was then ultrasonicated for 16 h to obtain a clear and stable suspension of YSZ nanoparticles in water. PS spheres with a diameter of 172 nm ± 6 nm and 295 nm ± 9 nm (Microparticles GmbH) were mixed with ultrapure water (resistivity of 18.2 MΩ cm) for further fabrication of full sphere PhGs (suspension pH adjusted to 2) and hollow sphere PhGs, respectively.

PhGs were produced by confined drop cast[27] of the suspensions inside polymer rings (inner Ø 2 cm) placed onto soda-lime glass substrates. The substrates were cleaned beforehand by 1 h sonication in a detergent solution (Mucasol 1%, Brand, Merz Hygiene GmbH), followed by brushing, rinsing with ultrapure water, and drying under nitrogen gas forced flow. The amount of drop casted suspension varied depending on the type of PhG to be produced. For PS full sphere PhGs, 150 μl of a suspension with concentration of 5 mg ml^{-1} was drop casted on previously heated substrates (60 °C). Drying was performed at this temperature and under atmospheric pressure for 15 min. For YSZ hollow sphere PhGs, deposition was performed according to our previously reported work.[49] A mixture of PS spheres of 295 nm size (13.8 mg ml^{-1}) and YSZ nanoparticles (5.5 mg ml^{-1}) in ultrapure water was prepared resulting in an YSZ/PS ratio of 0.4 by weight. The obtained suspension was ultrasonicated for 30 min (ultrasonic processor UP100H, Hielscher Ultrasonics), followed by drop cast of 70 μl of this homogenized suspension. The film was dried at ambient conditions. The PS template was removed by calcination in air at 500 °C for 30 min with a heating rate of 1 °C min^{-1}.

B. Measurements

The reflection spectra were measured using a spectrometer (cooled Carl Zeiss CCD spectrometer) integrated in the Carl Zeiss laser scanning microscope (Zeiss LSM 700), where 20× objective lens (200× magnification) was used. The measured area is 30 × 30 μm^2. Digital images are taken by using a normal camera. For color expression, the digital images of the PS full sphere PhG and the YSZ hollow sphere PhG are taken simultaneously to ensure the same conditions.

ACKNOWLEDGMENTS

The authors gratefully acknowledge financial support from the German Research Foundation (DFG) via SFB 986 "Tailor-Made Multi-Scale Materials Systems: M^3," Project Nos. C2, C4, and C5.

REFERENCES

[1] U. Osterwalder, M. Sohn, and B. Herzog, "Global state of sunscreens," Photodermatol., Photoimmunol. Photomed. **30**, 62 (2014).
[2] S. Kinoshita, S. Yoshioka, and J. Miyazaki, "Physics of structural colors," Rep. Prog. Phys. **71**, 76401 (2008).
[3] O. Ilic, P. Bermel, G. Chen, J. D. Joannopoulos, I. Celanovic, and M. Soljačić, "Tailoring high-temperature radiation and the resurrection of the incandescent source," Nat. Nanotechnol. **11**, 320 (2016).
[4] A. P. Raman, M. A. Anoma, L. Zhu, E. Rephaeli, and S. Fan, "Passive radiative cooling below ambient air temperature under direct sunlight," Nature **515**, 540 (2014).
[5] J. Wu, W. Liu, C. Xue, S. Zhou, F. Lan, L. Bi, H. Xu, X. Yang, and F.-D. Zeng, "Toxicity and penetration of TiO_2 nanoparticles in hairless mice and porcine skin after subchronic dermal exposure," Toxicol. Lett. **191**, 1 (2009).
[6] A. G. Dumanli and T. Savin, "Recent advances in the biomimicry of structural colours," Chem. Soc. Rev. **45**, 6698 (2016).
[7] M. Jansen and H. P. Letschert, "Inorganic yellow-red pigments without toxic metals," Nature **404**, 980 (2000).
[8] S. W. Kim, T. Hasegawa, M. Watanabe, K. Sugimoto, Y. Saito, K. Uematsu, K. Toda, and M. Sato, "Environmentally friendly Rb3V5O14 fluorescent red pigment," Dyes Pigm. **136**, 219 (2017).
[9] Y. Zhai, Y. Ma, S. N. David, D. Zhao, R. Lou, G. Tan, R. Yang, and X. Yin, "Scalable-manufactured randomized glass-polymer hybrid metamaterial for daytime radiative cooling," Science **355**, 1062 (2017).
[10] A. Kristensen, J. K. W. Yang, S. I. Bozhevolnyi, S. Link, P. Nordlander, N. J. Halas, and N. A. Mortensen, "Plasmonic colour generation," Nat. Rev. Mater. **2**, 16088 (2017).
[11] K.-T. Lee, C. Ji, D. Banerjee, and L. J. Guo, "Angular-and polarization-independent structural colors based on 1D photonic crystals," Laser Photonics Rev. **9**, 354 (2015).
[12] B.-H. Cheong, O. N. Prudnikov, E. Cho, H.-S. Kim, J. Yu, Y.-S. Cho, H.-Y. Choi, and S. T. Shin, "High angular tolerant color filter using subwavelength grating," Appl. Phys. Lett. **94**, 213104 (2009).
[13] K. Chung, S. Yu, C.-J. Heo, J. W. Shim, S.-M. Yang, M. G. Han, H.-S. Lee, Y. Jin, S. Y. Lee, N. Park, and J. H. Shin, "Flexible, angle-independent, structural color reflectors inspired by morpho butterfly wings," Adv. Mater. **24**, 2375 (2012).
[14] N. Vogel, S. Utech, G. T. England, T. Shirman, K. R. Phillips, N. Koay, I. B. Burgess, M. Kolle, D. A. Weitz, and J. Aizenberg, "Color from hierarchy: Diverse optical properties of micron-sized spherical colloidal assemblies," Proc. Natl. Acad. Sci. U. S. A. **112**, 10845 (2015).
[15] M. Xiao, Z. Hu, Z. Wang, Y. Li, A. D. Tormo, N. Le Thomas, B. Wang, N. C. Gianneschi, M. D. Shawkey, and A. Dhinojwala, "Bioinspired bright noniridescent photonic melanin supraballs," Sci. Adv. **3**, e1701151 (2017).
[16] H. Gu, Y. Zhao, Y. Cheng, Z. Xie, F. Rong, J. Li, B. Wang, D. Fu, and Z. Gu, "Tailoring colloidal photonic crystals with wide viewing angles," Small **9**, 2266 (2013).
[17] T. M. Choi, J.-G. Park, Y.-S. Kim, V. N. Manoharan, and S.-H. Kim, "Osmotic-pressure-mediated control of structural colors of photonic capsules," Chem. Mater. **27**, 1014 (2015).
[18] S.-H. Kim, S. Y. Lee, G.-R. Yi, D. J. Pine, and S.-M. Yang, "Microwave-assisted self-organization of colloidal particles in confining aqueous droplets," J. Am. Chem. Soc. **128**, 10897 (2006).
[19] P. Simonis and J. P. Vigneron, "Structural color produced by a three-dimensional photonic polycrystal in the scales of a longhorn beetle: Pseudomyagrus waterhousei (Coleoptera: Cerambicidae)," Phys. Rev. E **83**, 011908 (2011).
[20] S. Vignolini, P. J. Rudall, A. V. Rowland, A. Reed, E. Moyroud, R. B. Faden, J. J. Baumberg, B. J. Glover, and U. Steiner, "Pointillist structural color in Pollia fruit," Proc. Natl. Acad. Sci. U. S. A. **109**, 15712 (2012).
[21] D. P. Josephson, M. Miller, and A. Stein, "Inverse opal SiO_2 photonic crystals as structurally-colored pigments with additive primary colors," Z. Anorg. Allg. Chem. **640**, 655 (2014).
[22] C. I. Aguirre, E. Reguera, and A. Stein, "Colloidal photonic crystal pigments with low angle dependence," ACS Appl. Mater. Interfaces **2**, 3257 (2010).
[23] T. Brock, M. Groteklaes, and P. Mischke, *European Coatings Handbook* (Vincentz Network GmbH & Co KG, 2000).
[24] M. Elias, "Relationship between the size distribution of mineral pigments and color saturation," Appl. Opt. **50**, 2464 (2011).
[25] P. Liu, J. Chen, Z. Zhang, Z. Xie, X. Du, and Z. Gu, "Bio-inspired robust non-iridescent structural color with self-adhesive amorphous colloidal particle arrays," Nanoscale **10**, 3673 (2018).
[26] K. Katagiri, Y. Tanaka, K. Uemura, K. Inumaru, T. Seki, and Y. Takeoka, "Structural color coating films composed of an amorphous array of colloidal particles via electrophoretic deposition," NPG Asia Mater. **9**, e355 (2017).
[27] P. D. García, R. Sapienza, and C. López, "Photonic glasses: A step beyond white paint," Adv. Mater. **22**, 12 (2010).
[28] J. D. Forster, H. Noh, S. F. Liew, V. Saranathan, C. F. Schreck, L. Yang, J.-G. Park, R. O. Prum, S. G. J. Mochrie, C. S. O'Hern, H. Cao, and E. R. Dufresne, "Biomimetic isotropic nanostructures for structural coloration," Adv. Mater. **22**, 2939 (2010).
[29] M. Iwata, M. Teshima, T. Seki, S. Yoshioka, and Y. Takeoka, "Bio-inspired bright structurally colored colloidal amorphous array enhanced by controlling thickness and black background," Adv. Mater. **29**, 1605050 (2017).
[30] A. Kawamura, M. Kohri, G. Morimoto, Y. Nannichi, T. Taniguchi, and K. Kishikawa, "Full-color biomimetic photonic materials with iridescent and non-iridescent structural colors," Sci. Rep. **6**, 33984 (2016).
[31] Y. Takeoka, S. Yoshioka, A. Takano, S. Arai, K. Nueangnoraj, H. Nishihara, M. Teshima, Y. Ohtsuka, and T. Seki, "Production of colored pigments with amorphous arrays of black and white colloidal particles," Angew. Chem., Int. Ed. **52**, 7261 (2013).
[32] M. Xiao, Y. Li, M. C. Allen, D. D. Deheyn, X. Yue, J. Zhao, N. C. Gianneschi, M. D. Shawkey, and A. Dhinojwala, "Bio-inspired structural colors produced via self-assembly of synthetic melanin nanoparticles," ACS Nano **9**, 5454 (2015).
[33] Y. Zhang, B. Dong, A. Chen, X. Liu, L. Shi, and J. Zi, "Using cuttlefish ink as an additive to produce non-iridescent structural colors of high color visibility," Adv. Mater. **27**, 4719 (2015).
[34] M. Kohri, Y. Nannichi, T. Taniguchi, and K. Kishikawa, "Biomimetic non-iridescent structural color materials from polydopamine black particles that mimic melanin granules," J. Mater. Chem. C **3**, 720 (2015).
[35] D. Ge, E. Lee, L. Yang, Y. Cho, M. Li, D. S. Gianola, and S. Yang, "A robust smart window: Reversibly switching from high transparency to angle-independent structural color display," Adv. Mater. **27**, 2489 (2015).
[36] P. D. García, R. Sapienza, Á. Blanco, and C. López, "Photonic glass: A novel random material for light," Adv. Mater. **19**, 2597 (2007).
[37] S. G. Romanov, S. Orlov, D. Ploss, C. K. Weiss, N. Vogel, and U. Peschel, "Engineered disorder and light propagation in a planar photonic glass," Sci. Rep. **6**, 27264 (2016).
[38] H. Noh, S. F. Liew, V. Saranathan, S. G. J. Mochrie, R. O. Prum, E. R. Dufresne, and H. Cao, "How noniridescent colors are generated by quasi-ordered structures of bird feathers," Adv. Mater. **22**, 2871 (2010).
[39] S. Magkiriadou, J.-G. Park, Y.-S. Kim, and V. N. Manoharan, "Absence of red structural color in photonic glasses, bird feathers, and certain beetles," Phys. Rev. E **90**, 062302 (2014).
[40] G. Shang, L. Maiwald, H. Renner, D. Jalas, M. Dosta, S. Heinrich, A. Petrov, and M. Eich, " Photonic glass for high contrast structural color," Sci. Rep. **8**, 7804 (2018).
[41] L. Maiwald, S. Lang, D. Jalas, H. Renner, A. Y. Petrov, and M. Eich, "Ewald sphere construction for structural colors," Opt. Express **26**, 11352 (2018).
[42] M. Born and E. Wolf, *Principles of Optics: Electromagnetic Theory of Propagation, Interference and Diffraction of Light*, 7th ed. (Cambridge University Press, 1999).
[43] B. E. Warren, *X-Ray Diffraction* (Addison-Wesley Publishing Co, 1969).
[44] M. Ogurreck, J. J. do Rosario, E. W. Leib, D. Laipple, I. Greving, F. Marschall, A. Last, G. A. Schneider, T. Vossmeyer, H. Weller, F. Beckmann, and M. Müller,

"Determination of the packing fraction in photonic glass using synchrotron radiation nanotomography," J. Synchrotron Radiat. **23**, 1440 (2016).
[45]D. L. Wood and K. Nassau, "Refractive index of cubic zirconia stabilized with yttria," Appl. Opt. **21**, 2978 (1982).
[46]J.-G. Park, S.-H. Kim, S. Magkiriadou, T. M. Choi, Y.-S. Kim, and V. N. Manoharan, "Full-spectrum photonic pigments with non-iridescent structural colors through colloidal assembly," Angew. Chem., Int. Ed. **53**, 2899 (2014).
[47]R. W. G. Hunt and M. R. Pointer, *Measuring Colour* (John Wiley & Sons, 2011).
[48]C. Guiot, S. Grandjean, S. Lemonnier, J.-P. Jolivet, and P. Batail, "Nano single crystals of yttria-stabilized zirconia," Cryst. Growth Des. **9**, 3548 (2009).
[49]J. J. do Rosário, P. N. Dyachenko, R. Kubrin, R. M. Pasquarelli, A. Y. Petrov, M. Eich, and G. A. Schneider, "Facile deposition of YSZ-inverse photonic glass films," ACS Appl. Mater. Interfaces **6**, 12335 (2014).